Improved Power Quality On-Board Integrated Charger With Reduced Switching Stress

Jyoti Gupta, *Student Member, IEEE*, Rakesh Maurya, *Member, IEEE*, and Sabha Raj Arya, *Senior Member, IEEE*

***Abstract*—There is a consistent demand for reliable, efficient, small-sized, and light weight on-board chargers for vehicular battery charging applications. In view of aforesaid requirements, these chargers are restricted to Level-1 and Level-2 charging. Therefore, it leads to larger charging time. The proposed charger is integrated with propulsion machine drive system that serves to utilize the high power-rated electrical machine and motor-drive voltage source converter to facilitate vehicular battery charging when the vehicle is not running. This article presents mathematical modeling under various operational modes, analysis, and design considerations for the proposed system configuration. The entire system is developed in sim-power system toolbox of MATLAB software and tested in real-time implementation. The performance investigations of proposed charging system are carried out for vehicle battery charging under steady state as well as source variations. Furthermore, to ensure power quality features, total harmonic distortions of source voltage, and current and input power factor, are monitored. The salient features of proposed systems include no additional circuit, on-board charger suitable for fast charging, plugged in with single-phase, 230-V, 50-Hz outlet. It also offers a reduction in switch stress, reduced filter size, less ripple in current and voltage, and also improves the dynamic response.**

***Index Terms*—Electric vehicles, integrated battery charger, interleaved control, single phase charging, state-of-charge (SOC), three-level (TL) converter.**

I. Introduction

DUE to the more stringent regulations on emissions and fuel economy, global warming, and constraints on energy resources, the electric vehicles (EVs) and plug-in hybrid electric vehicles (PHEVs), have attracted more and more attention by vehicle manufactures, governments, and customers [1]–[3]. In order to develop low-cost and reliable EVs and PHEVs, the research and development primarily focused on battery technology, charging infrastructure motors, and drives applications [4]. Out of above, the charging infrastructure is one of the key factors for the successful operation of EVs/ PHEVs system. Discharging or charging performance of battery plays a crucial role in the development of electrical/hybrid vehicles. The charging time and lifetime of the battery are related to the Levels 1, 2, and 3 of battery charger characteristics [5], [6]. In general, vehicle owners are expected to charge their vehicle battery during overnight at home in a garage/parking by plugged in to a convenience outlet for Level 1 (slow) charging. On contrary, future developments focus on Level 2 (semifast) charging to provide ample power. Usually house hold outlet of 230-V, 50-Hz is used for both Levels 1 and 2 chargers. EV battery charger must ensure that the utility current is drawn with low distortion and at high power factor to maximize the real power available from a utility outlet [7]. Installation of most of the charging stations should comply with the guidelines prescribed by several standards such as IEEE-1547, SAE-J2894, IEC1000-3-2, and the U.S. National Electric Code 690, etc. [4], [5].

EV battery chargers are classified into on-board and off-board chargers with unidirectional and bidirectional power flow. Battery chargers connections are of two types within the vehicle (on-board) and outside the vehicle (off-board) [8]–[10]. For charging the battery, two charging connectors are accessible, i.e., standard J1772 connector for Level 1, and Level 2 charging station and a CHADeMO for Level 3 fast charging stations. Off-board is a fast charger that provides high power to dc outlets but its manufacturing cost is high. As compared to on-board charging, fast charging reduces the battery life considerably [11]. Unlike off-board, on-board chargers are lighter in weight, smaller in size and volume. Typically, two conversion stage of an on-board charger is a front-end ac–dc voltage source converter with unity power factor correction feature followed by a dc–dc converter [12], [13]. Achieving high power level with aforesaid chargers is very difficult because of its large passive components.

For unidirectional power flow, the vehicle batteries could be charged through a unidirectional charger but the injection of power back to the grid is not possible. These chargers typically utilize diode bridge rectifier with filter components and dc–dc converter [14]–[17]. Today, these types of chargers are being implemented in a single stage to limit weight, size, volume, and also losses.

The bidirectional charging system consists two stages of operation to improve power factor using PWM voltage source converter and regulate the battery current/voltage using bidirectional dc–dc converter [18]–[20]. The PWM scheme is used in drive-mode operation of the system to generate torque and desired motor speed. In the battery charging mode, the PWM scheme with current control is employed to charge the battery with unity power factor operation.While operating in charging and discharging modes, it should draw a sinusoidal current with minimum phase angle to improve reactive power and maximize

Manuscript received October 21, 2019; revised January 23, 2020; accepted March 4, 2020. Date of publication March 18, 2020; date of current version June 23, 2020. Recommended for publication by Associate Editor M. Ferdowsi. *(Corresponding author: Rakesh Maurya.)*

The authors are with the Department of Electrical Engineering, Sardar Vallabhbhai National Institute of Technology, Surat 395007, India (e-mail: jgupta973@gmail.com; rmaurya@eed.svnit.ac.in; sabharaj94@gmail.com).

Color versions of one or more of the figures in this article are available online at https://ieeexplore.ieee.org.

Digital Object Identifier 10.1109/TPEL.2020.2981955

active power. This circuit provides fast controlling and high power density as compared to unidirectional charger, which accounts more components, more cost and greater challenge for implementation [21]–[23].

To reduce size, weight, and cost, windings of electric motor, inverter, and other hardware components are utilized for charging system, thus, integrated drive system with battery charger topology have been introduced. During charging process, few mandatory features of integrated on-board chargers are less harmonic content in supply current, unity power factor operation and there is no development of unwanted torque in motor.

This article focuses on single-phase on-board integrated charging system along with three-level bidirectional dc–dc converter topology. As compared to conventional dc–dc bidirectional converter, size requirements of filter inductor are considerably less in three-level bidirectional converter. Additionally, switch voltage stress is also reduced to half of the input dc-link voltage. Therefore, the dynamic response of integrated system is also superior to its counterpart [24]–[28].

This article starts with brief description of issues and challenges associated with EVs/ PHEVs. The description of integrated charging system is presented in Section II. Section III includes steady-state operating details of proposed converter under various switching modes. The control algorithms scheme for interleaved boost converter and three-level dc–dc converter are presented in Section IV. The design considerations of system configuration are described in Section V. The on-board integrated system of 8-kW, 400-V/20-A is developed using Simulink and sim-power system toolbox of MATLAB software and its testing in real-time implementation are discussed in Section VI. Section VII presents the comparative study of three-level dc–dc converter in buck mode over conventional buck converter to show its effectiveness. Finally, Section VIII concludes this article.

II. System Description of Integrated On-Board Charger

Fig. 1(a) shows the schematic diagram of on-board integrated drive system with battery charger topology. This system includes single-phase ac source (230 V, 50 Hz) as house hold outlet, electric motor, voltage source converter (VSC), control system, bidirectional dc–dc converter, and battery pack. Under propulsion mode of vehicle, the J1772 connector is opened and battery pack delivers power to electric motor via bidirectional dc–dc converter and three-phase VSC as demanded by the operating conditions of vehicle. In charging mode electric motor is at standstill and J1772 connector is closed. The stator windings of motor are used as filter inductors, three-phase VSC serves as a bidirectional ac–dc converter as depicted in Fig. 1(a).

The power circuit mainly consists of two parts namely interleaved boost converter (IBC) and three-level bidirectional dc–dc converter. The IBC comprises of stator windings of three-phase induction motor as three inductors (L_1, L_2, L_3), three-leg voltage source converter (VSC), split dc-link capacitors (C_1, C_2), and bidirectional three level dc–dc converter with power switches (Sw_1–Sw_4) and passive filters (*L, C),* as shown in Fig. 1(b).

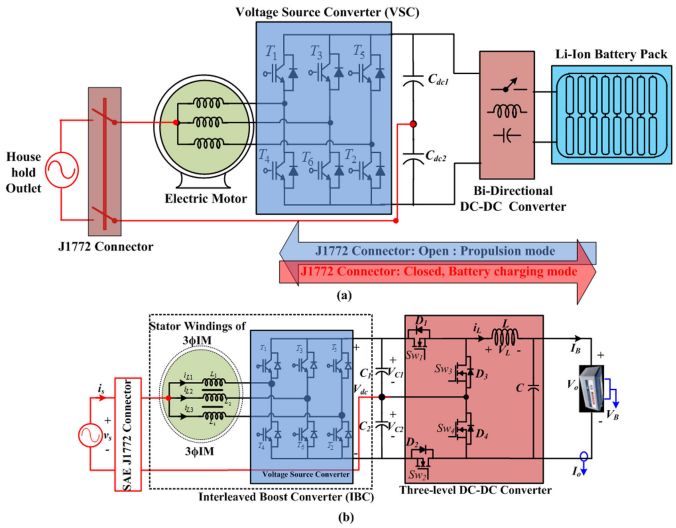

Fig. 1. Integrated on-board charger. (a) Schematic diagram. (b) Power topology.

During charging mode, single phase ac voltage (v_s) is applied to interleaved boost converter after closing SAE J1772 connector. The currents (i_{L1}, i_{L2}, i_{L3}) through inductors (L_1, L_2, L_3) are unidirectional in nature, and therefore, no electromagnetic torque is developed by the motor. Thus, rotor is at standstill condition. It is predictable to have unity power factor operation, requirement of reduced switching frequency of VSC, low source current harmonic distortion due to interleaved control of three-leg VSC connected stator windings.

The rectified output voltage (V_{dc}) of VSC is divided in two equal parts using split dc link capacitors (C_1, C_2) and fed to three-level bidirectional dc–dc converter. It is now be used for conditioning the dc voltage/ current to a constant voltage (CV)/ constant current (CC) for charging the vehicle battery. Fig. 1(b) shows three-level bidirectional dc–dc converter with four switches operates as *buck* converter. In this mode, two switches (Sw_1, Sw_2) operate with switching signals and switches (Sw_3, Sw_4) in OFF condition. Main attributes of three level dc–dc converter include reduced switch voltage stress, reduced filter size, and improved transient response.

III. Steady-State Operation

In this section, the steady-state operation under varying duty ratio control is presented using switching waveforms and its equivalent circuits under various operational modes. Prior to steady-state analysis, power switching devices, and all passive components are assumed to be lossless.

A. Operation of Interleaved Boost Converter

It is further assumed that for a given sampling time (T_s), supply voltage (v_s) remains constant. The duty ratio (d) of switches (T_1 to T_6) varies for each sampling time as supply voltage (v_s) keeps on varying sinusoidal. As shown in Fig. 2(a), in each sampling time, the switches (T_1, T_3, T_5) are ON for dT_{s1} and switches (T_4, T_6, T_2) are ON for $(1-d)T_{s1}$ period, where

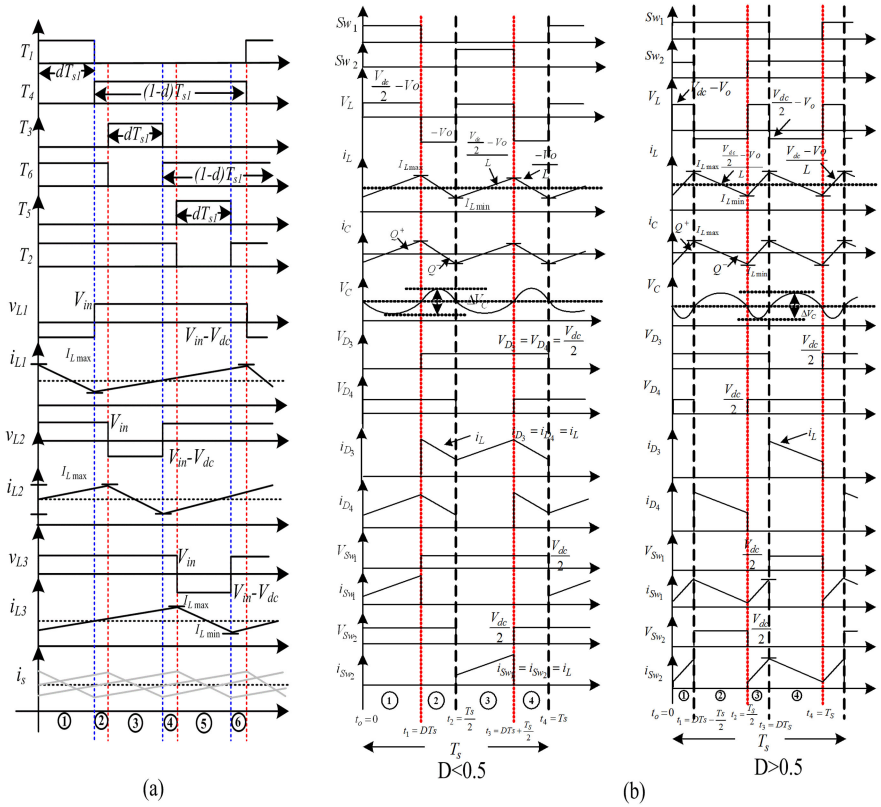

Fig. 2. Switching waveforms of onboard charger under one switching cycle. (a) IBC. (b) TL buck converter with duty ratio D $<$ 0.5 and D $>$ 0.5.

T_{s1} is switching period for switches of IBC. Depending upon the switching state of switches (T_1–T_6), six operating modes are identified, as shown in Fig. 2(a). These operating modes repeat several times in one cycle of the line frequency (i.e., 50/60 Hz). This interleaved boost converter works satisfactory when dc-link voltage ($V_{\rm dc}$) is more than peak of supply voltage (v_s) and operation is restricted in CCM mode only. The waveforms of voltage and current of filter inductors (L_1, L_2, L_3) are also depicted in Fig. 2(a). The inductor currents (i_{L1}, i_{L2}, i_{L3}) increase from their respective initial value whenever voltage across the concerned inductors are positive by turning ON switches (T_4, T_6, T_2), as shown in Fig. 2(a). Therefore, this mode is call as inductor charging mode. The inductor current decreases linearly with turning on of switches (T_1, T_3, T_5). It is observed that individual filter current has high ripple. However, the source current (i_s) contains lower ripple due to phase shifted operation of each leg of IBC.

B. Operation of Three-Level DC–DC Converter

Depending upon the desired charging voltage/current, the duty ratio (D) of power switches (Sw_1, Sw_2) of three-level bidirectional dc–dc converter (operate as buck operation) may varies either less than 0.5 or more than 0.5. In both values of D, the switches are controlled to regulate output voltage/ current to its desired value. The switching waveform over one switching cycle with D $<$ 0.5 and D $>$ 0.5 are shown in Fig. 2(b).

Case-I: Buck operation with D $<$ 0.5

During buck operation, the switches (Sw_3, Sw_4) are always off and its body diodes (D_3, D_4) are operational as per circuit conditions. The equivalent circuit during all possible switching state of TL dc–dc converter is shown in Fig. 3. Detailed analysis of dc–dc converter under both possible conditions (D $<$ 0.5 and D $>$ 0.5) is presented as follow.

1) Mode-I [t_0, t_1]: At instant $t = t_0$, switch Sw_1 turns ON and body diode D_4 conducts. Switch Sw_2 and body diode D_3 of switch Sw_3 are in OFF state. The equivalent circuit showing current path is depicted in Fig. 3(b). The voltage across Sw_2 and D_3 are $V_{\rm dc}/2$. The inductor current (i_L) increases from its initial value, as shown in Fig. 2(b). The voltage and current equations are as follows:

$$V_L = \frac{V_{\rm dc}}{2} - V_o;\ V_{Sw2} = V_{D3} = \frac{V_{\rm dc}}{2};\ V_{Sw1} = V_{D4} = 0$$

$$i_L = i_c + I_o;\ i_{Sw2} = i_{D3} = 0;\ i_{Sw1} = i_{D4} = i_L$$

$$i_L(t) = \frac{\frac{V_{\rm dc}}{2} - V_o}{L}(t - t_0) + i_L(t_0). \tag{1}$$

At the end of mode-I, maximum inductor current ($i_L(t_1) = I_{L\max}$) is obtained by substituting $i_L(t_o) = I_{L\min}$ and $t = DT_s$, in (1)

$$I_{L\max} = \frac{\frac{V_{\rm dc}}{2} - V_o}{L} DT_s + I_{L\min}. \tag{2}$$

2) Mode-II [t_1, t_2] and Mode-IV [t_3, t_4]: At instant $t_1 = DT_s$, switch Sw_1 turned OFF, and Sw_2 still remains OFF.

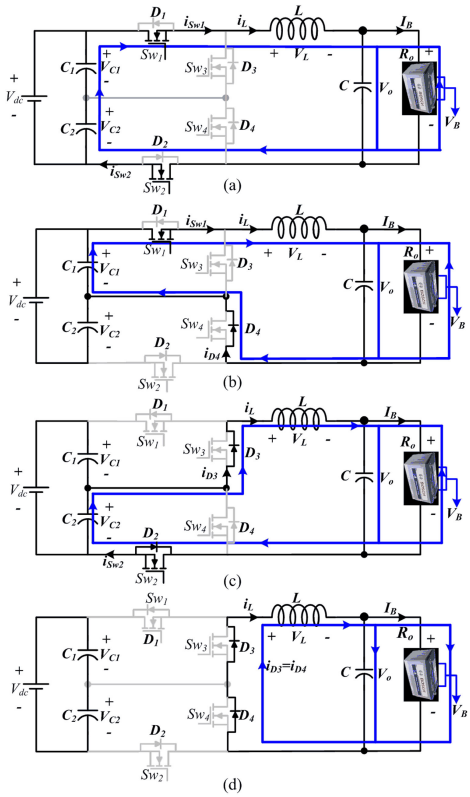

Fig. 3. Equivalent circuit during various mode of operation under one switching cycle.

The voltage stress across both switches is $V_{\rm dc}/2$. Inductor current freewheels through body diodes (D_3, D_4). The equivalent circuit showing current path is depicted in Fig. 3(d). The operation of dc–dc converter in mode-II is same as mode-IV. The voltage and current equations are as follows:

$$V_L = -V_o;\ V_{D3} = V_{D4} = 0;\ V_{Sw1} = V_{Sw2} = \frac{V_{\rm dc}}{2}$$
$$i_{D3} = i_{D4} = i_L;\ i_L = i_c + I_o;\ i_{Sw1} = i_{Sw2} = 0$$
$$i_L(t) = \frac{-V_o}{L}(t - t_1) + i_L(t_1). \tag{3}$$

Under steady-state condition, at the end of mode-II the value of inductor current is same as initial value ($i_L(t_2) = I_{L\min}$). It can be obtained by substituting $t_1 = DT_s$, $t = T_s/2$, in (3)

$$I_{L\min} = \frac{-V_o}{L}\left(\frac{T_s}{2} - DT_s\right) + I_{L\max}. \tag{4}$$

3) Mode-III [t_2, t_3]: At instant $t_2 = T_s/2$, switch Sw_2 turned ON and Sw_1 still remains OFF. Diode D_3 still remains on and D_4 becomes turned OFF. The voltage across Sw_1 and D_4 is $V_{\rm dc}/2$. For this time interval Sw_2 and D_3 are ON, as shown in Fig. 3(c). The voltage and current equations are as follows:

$$V_L = \frac{V_{\rm dc}}{2} - V_o;\ V_{Sw2} = V_{D3} = 0;\ V_{Sw1} = V_{D4} = \frac{V_{\rm dc}}{2}$$
$$i_L = i_c + I_o;\ i_{D3} = i_{Sw2} = i_L;\ i_{Sw1} = i_{D4} = 0$$
$$i_L(t) = \frac{\frac{V_{\rm dc}}{2} - V_o}{L}(t - t_2) + i_L(t_2). \tag{5}$$

At the end of mode-III, the value inductor current is obtained by Substituting $t_2 = T_s/2$, $t = DT_s + T_s/2$, in (5)

$$I_{L\max} = \frac{\frac{V_{\rm dc}}{2} - V_o}{L} DT_s + I_{L\min}. \tag{6}$$

Case-II: Buck operation with D > 0.5

Depending on desired voltage for battery charging, the value of duty ratio, D may be more than 0.5. Therefore, analysis of TL dc–dc converter is also carried out as given below. In this case, switching waveforms of voltage and current are depicted in Fig. 2(b).

4) Mode-I [t_0, t_1] and Mode-III [t_2, t_3]: In these modes, both the switches Sw_1 and Sw_2 are in on state and the body diodes D_3 and D_4 are in reversed biased. The inductor current (i_L) increases from its initial value are shown in Fig. 2(b). The operation of dc–dc converter in mode-III is same as mode-I. The voltage, current equations are as follows:

$$V_L = V_{\rm dc} - V_o;\ V_{D3} = V_{D4} = \frac{V_{\rm dc}}{2};\ V_{Sw1} = V_{Sw2} = 0$$
$$i_L = i_C + I_o;\ i_{D3} = i_{D4} = 0;\ i_{Sw1} = i_{Sw2} = i_L$$
$$i_L(t) = \frac{V_{\rm dc} - V_o}{L}(t - t_0) + i_L(t_0). \tag{7}$$

At the end of mode-I, the value of inductor current can be obtained by substituting to = 0, t = DTs-Ts/2, in (7)

$$I_{L\max} = \frac{V_{\rm dc} - V_o}{L}\left(DT_s - \frac{T_S}{2}\right) + I_{L\min}. \tag{8}$$

5) Mode-II [t_1, t_2]: At instant $t_1 = DT_s - T_s/2$, Sw_1 still remains on but Sw_2 is turned OFF. The equivalent circuit showing current path is depicted in Fig. 3(b). This mode operation is same as Mode-I of case D < 0.5 operation.

6) Mode-IV [t_3, t_4]: At instant $t_3 = DT_s$, switch Sw_1 turned OFF and Sw_2 still remains ON. This mode operation analysis is same as mode-III of D < 0.5 case.

IV. Control Algorithm Scheme

In order to regulate dc-link voltage and simultaneously charge the vehicle battery as per CV and CC modes, two control schemes are implemented. First, an interleaved control algorithm for IBC to maintain constant dc-link voltage ($V_{\rm dc}$) along with unity power factor operation. Second, regulation of output voltage (V_o)/output current (I_o) of bidirectional three-level dc–dc converter to maintain a constant voltage/constant current value in charging mode. The details of each control algorithm are given as follows.

A. Control Algorithm for Interleaved Boost Converter

In order to understand the interleaved control algorithm for power factor corrected IBC, it is assumed that for a specified sampling time (T_s), supply voltage (v_s) remains constant V_{in}. The duty ratio (d) of power switches (T_1–T_6) varies for each sampling as supply voltage (v_s) keeps on changing. Each leg of IBC operates with equal phase shift of $T_s/3$. where T_s is switching period for power switches (T_1–T_6).

Fig. 4(a) shows split dc voltage controller technique for maintaining the midpoint voltage zero. Through this technique used

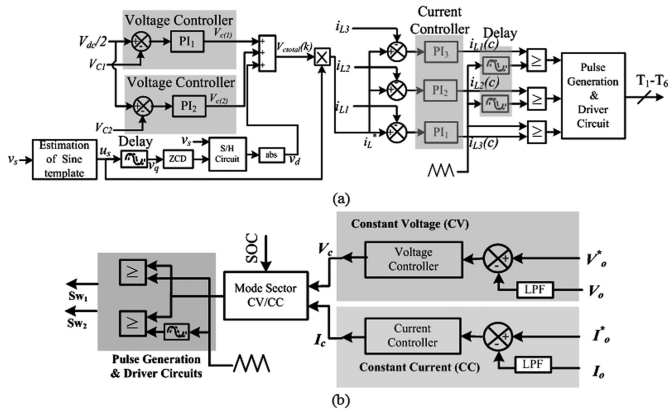

Fig. 4. Schematic diagram of control system. (a) Interleaved control algorithm for IBC. (b) Control algorithm for three-level dc–dc converter.

two identical proportional-integral (PI) controller to maintain the equality of capacitor voltage V_{C1} and V_{C2}. In this scheme desired voltage $V^*_{\rm dc}/2(k)$ is compared with the sensed dc-link voltage $V_{C1}(k)$, to make a voltage error $V_e(k)$, at any instant "*k*" as given below [27]. The voltage error $V_e(k)$ is fed to first voltage controller (PI_1) for generation of a controlled output $V_c(1)(k)$, as given in (10), where K_{pv1}, K_{iv1} are the proportional gain and integral gain of the first voltage controller

$$V_e(k) = \frac{V^*_{\rm dc}}{2}(k) - V_{C1}(k)$$
$$V_c(1)(k) = V_c(1)(k-1) + K_{pv1}\{V_e(k) - V_e(k-1)\} + K_{iv1}V_e(k). \quad (9)$$

For second PI controller (PI_2), to maintain V_{C2}, equations same as (9) are developed, where, K_{pv2}, K_{iv2} are the proportional gain and integral gain of the second voltage controller

$$V_e(k) = \frac{V^*_{\rm dc}}{2}(k) - V_{C2}(k)$$
$$V_c(2)(k) = V_c(2)(k-1) + K_{pv2}\{V_e(k) - V_e(k-1)\} + K_{iv2}V_e(k). \quad (10)$$

Fig. 4(a) used zero crossing detector and sample and hold circuit to get the d-component of input supply voltage from sine template of input sinusoidal voltage. The total output generates after adding three outputs of two PIs and d-component of supply voltage. The peak value (V_m) of single-phase ac source can be computed as follows [26]:

$$V_m = \sqrt{{v_d}^2 + {v_q}^2} \quad (11)$$

where $v_d = V_m \sin\omega t$ and $v_q = V_m \sin(\omega t - 90)$ are the components in-phase and quadrature of ac supply voltage. The components (v_d, v_q) of supply voltage (v_s) can be generated from phase shifting block, which is inbuilt in estimation of sine template block of Fig. 4(a).

The unit template of supply voltage $u_s(k)$ is derived as follows:

$$u_s(k) = \frac{v_d}{V_m}. \quad (12)$$

The reference current $i^*_L(k)$ is obtained by multiplying the total output of split dc-bus controller technique $V_{\rm ctotal}(k)$ [27], with the unit template of $u_s(k)$as follows:

$$i^*_L(k) = u_s(k)V_{\rm ctotal}(k). \quad (13)$$

This reference current $i^*_L(k)$ is compared with the sensed inductor currents (i_{L1}, i_{L2}, i_{L3}) and passed through individual current controller (PI_1, PI_2, PI_3). The output signal of individual current controller is represented by

$$i_{L1c}(k) = i_{L1c}(k-1) + K_{pLc}\{i_{e1}(k) - i_{e1}(k-1)\} + K_{iLc}i_{e1}(k)$$
$$i_{L2c}(k) = i_{L2c}(k-1) + K_{pLc}\{i_{e2}(k) - i_{e2}(k-1)\} + K_{iLc}i_{e2}(k)$$
$$i_{L3c}(k) = i_{L3c}(k-1) + K_{pLc}\{i_{e3}(k) - i_{e3}(k-1)\} + K_{iLc}i_{e3}(k) \quad (14)$$

where K_{iLc} and K_{pLc} are, respectively, the integral and proportional gain and are same for three PI current controllers. The output signal of each current controller is compared with phase shifted triangular wave of frequency 2.5 kHz to generate the PWM signals for switches (T_1–T_6) of IBC converter, as shown in Fig. 4(a). The ripple content in supply current is significantly used due to interleaved operation of each leg.

B. Control Algorithm for Three-Level DC–DC Converter

During charging mode, three-level bidirectional dc–dc converter works as buck operation in which power switches (Sw_1, Sw_2) operate as interleaved control, i.e., phase shifted 90° to lessen filter inductor and capacitor size significantly. The TL-buck converter operates under constant voltage/ constant current modes as per battery state-of-charge (SOC). Here, Fig. 4(b) shows schematic diagram of constant voltage/current control algorithm applied to charge the battery.

When SOC of battery is low (below 30%), the constant current charging is applied by mode selector block of Fig. 4(b). In this control scheme, output current (I_o) is compared with desired current I^*_o at any instant "*k*" to generate error in current $I_e(k) = I^*_o(k) - I_o(k)$. This error signal is fed to PI controller for generation of controlling the current $I_c(k)$, as given in

$$I_c(k) = I_c(k-1) + K_{\rm pcc}\{I_e(k) - I_e(k-1)\} + K_{\rm icc}I_e(k) \quad (15)$$

where $K_{\rm icc}$ and $K_{\rm pcc}$ are, respectively, the integral and proportional gain of PI current controller.

When SOC of battery reaches to 73%, the constant voltage charging mode is selected by mode selector block. Similar to constant current charging mode, this mode is accomplished by comparing output voltage (V_o) with desired voltage and voltage error signal, $V_e(k) = V^*_o(k) - V_o(k)$ is generated at any instant k. This error signal is fed to voltage controller to obtain controlled voltage $V_c(k)$, as given in

$$V_c(k) = V_c(k-1) + K_{\rm pcv}\{V_e(k) - V_e(k-1)\} + K_{\rm icv}V_e(k) \quad (16)$$

where $K_{\rm icv}$ *and* $K_{\rm pcv}$, respectively, are the integral and proportional gain of PI voltage controller. Amplified signals, $V_c(k)$ and $I_c(k)$ are compared with phase shifted saw-tooth carrier signals of 10 kHz for generating the switching signals for switches. These switching signals are connected to driver circuits of power switches (Sw_1, Sw_2).

V. Design Considerations

The design of system for integrated battery charger includes mainly selection of circuit parameters of interleaved boost converter (IBC) such as selection of filters (L_1, L_2, L_3) and dc-link capacitors (C_1, C_2) and that of three-level dc–dc converter such as inductor (L) and capacitor (C).

A. Selection of Circuit Parameters of IBC

It is designed to provide regulated dc-link voltage ($V_{\rm dc}$) along with power factor correction at the ac supply mains. The values of filter inductors (L_1, L_2, L_3) are selected such that IBC operates in CCM in all operating conditions. The design equations of filters (L_1, L_2, L_3) and dc-link capacitors (C_1, C_2) are given in [28]

$$I_{pk} = \frac{\sqrt{2}P_{\rm in}}{V_{\rm in}}; V_{\rm dc} = \frac{1}{(1-D_{\rm min})}V_{\rm in} \tag{17}$$

where $V_{\rm in} = \sqrt{2}V_s$ and $V_s =$ rms Value of supply voltage (v_s)

$$L_{i\,\rm min} = \frac{\sqrt{2}V_{\rm in}D_{\rm min}}{f_{Sw}\Delta I};\ i = 1,2,3$$
$$C_1 = C_2 = \frac{D}{R\frac{\Delta V_{\rm dc}}{V_{\rm dc}}f_s}. \tag{18}$$

The calculated minimum value of filters ($L_1 = L_2 = L_3$) and dc-link capacitor (C_1, C_2) are 5.6 mH and 8852 μF at switching frequency (f_s) 2.5 kHz, 30% ripple in input current, and 1% ripple in dc-link voltage. The consider design values of aforesaid components are given in Appendix A.1.

B. Selection of Circuit Parameters of Three-Level DC–DC Converter

It is designed to provide regulated dc output voltage/current as required by battery charging applications. The values of inductor (L) and output capacitor (C) are selected such that three-level dc–dc converter operates in CCM mode during battery charging.

1) Voltage Conversion Ratio: For periodic operation of dc–dc converter, the average of inductor voltage should be zero. Express the average of inductor voltage over one switching cycle as follows:

$$\left(\frac{V_{\rm dc}}{2} - V_o\right)DT_s - V_o\left(\frac{T_S}{2} - DT_s\right) = 0\,;\ D < 0.5$$
$$(V_{\rm dc} - V_o)\left(DT_s - \frac{T_S}{2}\right) + \left(\frac{V_{\rm dc}}{2} - V_o\right)(T_S - DT_s) = 0\ ;D > 0.5. \tag{19}$$

Solving (19) for both the case of duty ratio, yields

$$\frac{V_o}{V_{\rm dc}} = D. \tag{20}$$

The voltage conversion ratio of three-level buck mode converter is the same as that in the conventional buck converter.

2) Design of Output Inductor (L): Assuming that the average power supplied by the dc link and absorbed by the load must be same that will determine the average output inductor current. Therefore, output inductor current average value is evaluated as

$$i_L = I_O = \frac{V_0}{R_o} = \frac{DV_{\rm dc}}{R_o}. \tag{21}$$

Average value of output inductor current (I_L) is same for $D < 0.5$ and $D > 0.5$, as shown in (21). Thus, For D < 0.5 the maximum and minimum value of output inductor currents are determined by using (8), (20), and (21), which are given as follows:

$$I_{L\,\max} = \frac{V_o}{R_o} + \frac{V_o(1-2D)}{4fL}$$
$$I_{L\,\min} = \frac{V_o}{R_o} - \frac{V_o(1-2D)}{4fL};\ D < 0.5. \tag{22}$$

For ($D > 0.5$) max and min value output inductor currents are determined by using (14), (20), and (21), given as follows:

$$I_{L\,\max} = \frac{V_o}{R_o} + \frac{V_o\,(1-D)\,(2D-1)}{4fLD}$$
$$I_{L\,\min} = \frac{V_o}{R_o} - \frac{V_o\,(1-D)\,(2D-1)}{4fLD};\ D > 0.5. \tag{23}$$

For the converter to operate in CCM mode, the min value of output inductor current has to be positive. Therefore, the boundary condition between continuous and discontinuous mode of inductor current is determined from (22) and (23) within $I_{L\rm min} = 0$. Thus, min value of output inductor $L_{\rm crit}$ for continuous mode of current in the converter is calculated by using

$$L_{\rm crit} = \frac{(1-2D)R_o}{4f}\ ;\ D < 0.5$$
$$L_{\rm crit} = \frac{(2D-1)(1-D)R_o}{4Df}\ ;D > 0.5. \tag{24}$$

3) Design of Output Capacitor (C): To keep the constant output voltage, capacitor value should to be very large. But in practice, the capacitor output voltage cannot be kept completely constant with a finite value of capacitance. The variation in capacitor output voltage and ripple in output voltage are computed from the voltage and current relation of capacitor. The capacitor current during switching is $i_c = i_L - I_o$. At the time of capacitor charging, the output capacitor current must be positive.

The change in charge ΔQ is determined by the area of the triangle shown in Fig. 3(b) and is written as

$$\Delta Q = C\Delta V_O = \frac{1}{2}\left(\frac{\Delta i_L}{2}\right)\left(\frac{T}{4}\right) = \frac{\Delta i_L T_s}{16}. \tag{25}$$

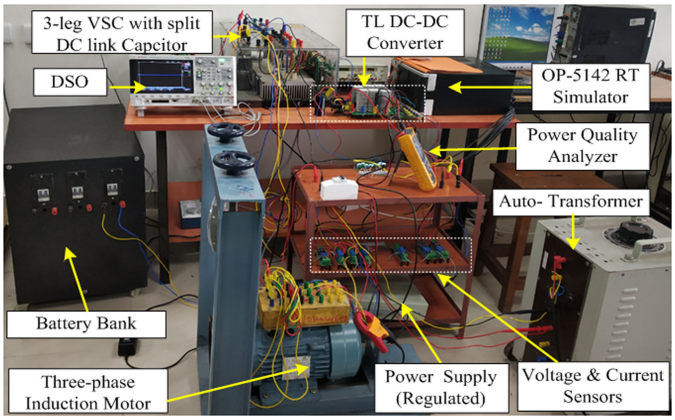

Fig. 5. Photograph of a prototype integrated EV battery charger.

Expression of output capacitor (C) can be obtained by solving (22), (26) and (23), (26), and written as

$$C = \frac{\Delta i_L T_s}{16 \Delta V_o}. \tag{26}$$

An estimated expression for the essential value of capacitance as a function of ripple voltage constraint ΔV_o, duty ratio D, switching frequency f, and output voltage V_o is specified as

$$C = \frac{(1-2D)}{32 f^2 L \left(\frac{\Delta V_0}{V_o}\right)} \; ; \; D < 0.5$$

$$C = \frac{(1-D)(2D-1)}{32 D f^2 L \left(\frac{\Delta V_0}{V_o}\right)}; D > 0.5. \tag{27}$$

Considering the equivalent series resistance (ESR) for the accurate design of output value of capacitor can be carried out in the ripple of output voltage ΔV_o. Normally, ESR value is designed by manufacturer. However, the effective value of equivalent series inductance (ESL) below 100 kHz can be neglected. The output voltage ripple with ESR be given as

$$\Delta V_o = \frac{\Delta i_L T_s}{16 C} + \Delta I_c r_{c_o}. \tag{28}$$

Based on the aforementioned designed (20)–(28), 8-kW, 400-V/20-A, on-board integrated system for charging vehicle battery is developed. Selected parameters for experimental study are given in Appendix.

VI. Results and Discussions

The on-board integrated charging system of 8-kW, 400-V/20-A is developed using Simulink and sim-power system toolbox of MATLAB Software and its performances are investigated. To validate the system performance, a prototype of same specification is built in the laboratory environment, as depicted in Fig. 5.

The three-level bidirectional dc–dc converter in charging mode with integrated system and its control algorithm is programmed in FPGA-based XC3S5000 series processor using OP-5142 real-time simulator with real-time sampling frequency of 50 μS. A Fluke make power quality analyzer in single phase

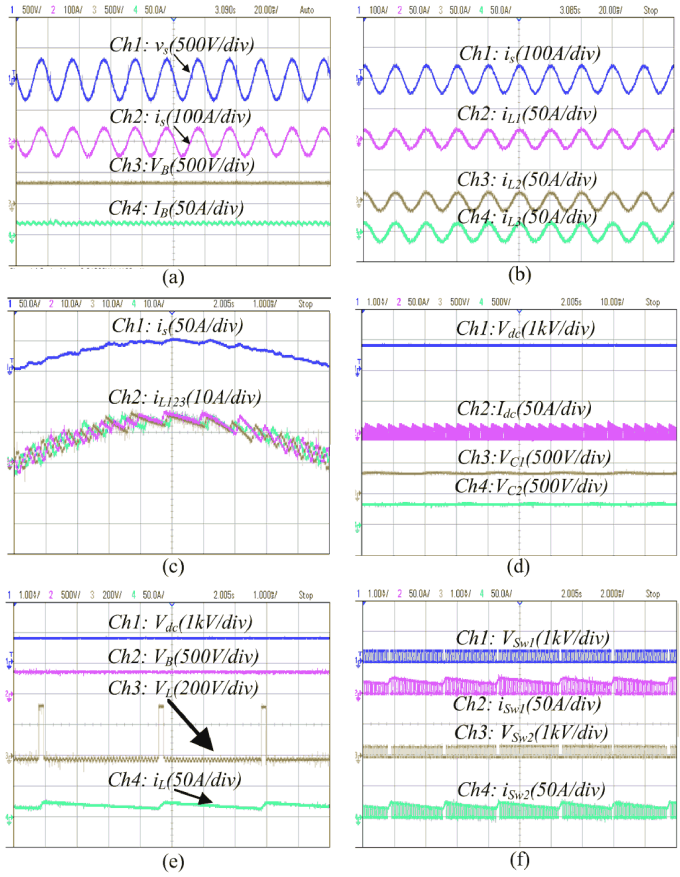

Fig. 6. Experimental performance of steady state voltage and current waveforms of bidirectional integrated system in charging mode feeding 8 kW power to battery load in CC mode at source voltage of 230 V.

(43B) and Agilent make four channel DSO-X-2004A digital oscilloscope are used to measure test waveforms under steady state and dynamic conditions, respectively. The performance of integrated system with battery charging applications is observed for constant voltage and constant current mode.

A. Steady-State Performance of Integrated Charging System at 230 V in CV and CC Mode

Source voltage (v_s), source current (i_s), filter inductor currents (i_{L1}, i_{L2}, i_{L3}), dc-link voltage (V_{dc}), and dc-link current (I_{dc}) are measured at input supply and dc link side of integrated system in Fig. 6. Also, in order to investigate the performance of three-level bidirectional dc–dc converter of integrated system, switch voltage (V_{Sw}), switch current (i_{Sw}), output inductor voltage (V_L), and output inductor current (i_L) in charging mode are also observed with the battery voltage and current (V_B, I_B) Figs. 6 and 7 show the steady-state results at supply voltage of 230 V in CC and CV charging modes.

It is observed that Fig. 6(a) shows source voltage and current are in same phase, battery voltage of 362 V, and battery current of 20 A. With wide range of variation in supply voltage, battery current is maintained constant in constant current mode with 30% of initial SOC.

In constant current mode battery is charging with 20 A constant current and the battery output voltage is unregulated.

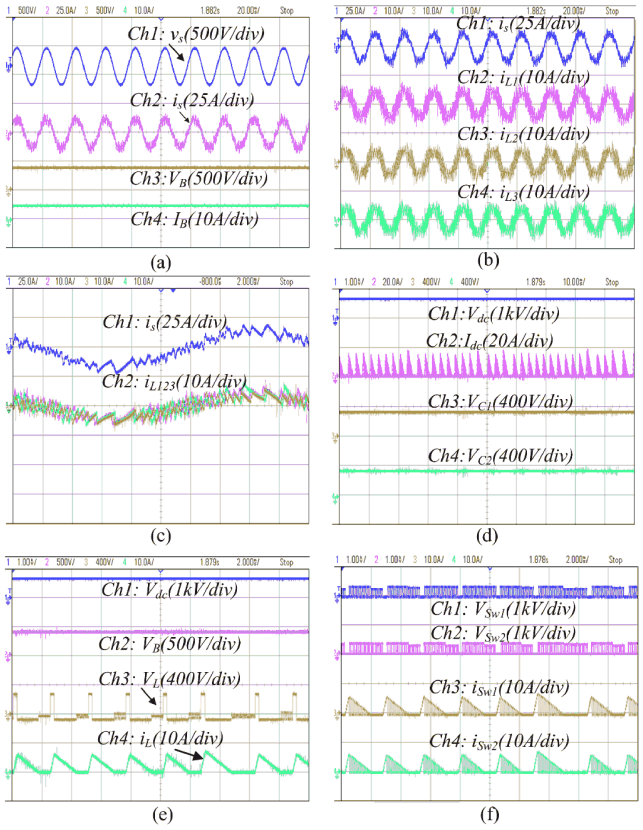

Fig. 7. Experimental performance of steady state voltage and current waveforms of bidirectional integrated system in charging mode feeding 2 kW power to battery load in CV mode at source voltage of 230 V.

Fig. 6(b) presents individual inductor current at input side, Fig. 6(c) shows interleaved control at input side of inductor current. Fig. 6(d) shows 700 V dc-link voltage and voltage across each input capacitors C_1 and C_2, i.e., 350 V. Fig. 6(e) shows output inductor voltage and current, battery voltage of 362 V. Fig. 6(f) shows switch stress 350 V, i.e., half of input voltage of bidirectional three level converter of integrated system. Fig. 7(a)–(f) show voltage and current waveforms in same steady-state condition for charging the battery in constant voltage mode with 230 V supply voltage. As per practice, when battery charged reaches to 70 to 80% of SOC, at this SOC value three level bidirectional dc–dc converter fed power for charging battery shifted to CV mode.

In constant voltage mode, minimum power of 2 kW is provided to charge battery with 5 A current. The battery charging with constant output voltage of 400 V and battery voltage 374 V when SOC is above 73%. Fig. 6(d)–(f) and Fig. 7(d)–(f) show dc-link voltage, voltage across each input capacitor (C_1, C_2), switching voltage values are same in both the modes (CV and CC). When battery SOC shifted to 73% input current is reduced from 20 to 5 A and input inductor current value also reduced from 56 to 18 A. In CV mode, Fig. 7(b) shows distortion in supply current is more as compare to CC mode. Fig. 7(e) shows discontinuous current flowing through inductor in CV mode but it is continuous in nature shown in Fig. 6(e) for CC mode. For worst case situation supply voltage of 85 V, system performance

TABLE I
POWER QUALITY INDICES OF BATTERY CHARGING WITH DIFFERENT SUPPLY VOLTAGES

Supply Voltage V_s (V)		Battery Charging Modes: Constant Voltage Mode V_{sTHD} (%)	i_{sTHD} (%)	PF	Constant Current Mode V_{sTHD} (%)	i_{sTHD} (%)	PF
85	Sim.	0	3.62	0.97	0	1.62	0.98
	Exp.	0.8	2.1	1	0.6	0.6	1
120	Sim.	0	3.87	0.97	0	1.24	0.98
	Exp.	0.5	3.2	0.99	0.5	1.2	0.99
150	Sim.	0	7.83	0.97	0	1.73	0.99
	Exp.	0.5	5.4	0.99	0.5	2.1	0.99
180	Sim.	0	8.48	0.95	0	3.17	0.99
	Exp.	0.3	7.4	0.98	0.4	2.8	1
200	Sim.	0	9.59	0.96	0	4.31	0.99
	Exp.	0.3	8.2	0.98	0.4	3.4	1
230	Sim.	0	9.24	0.96	0	3.99	0.99
	Exp.	0.3	9.7	0.98	0.3	3.0	1
265	Sim.	0	56.6	0.95	0	14.6	0.97
	Exp.	0.3	47.4	0.95	0.3	13.3	0.99

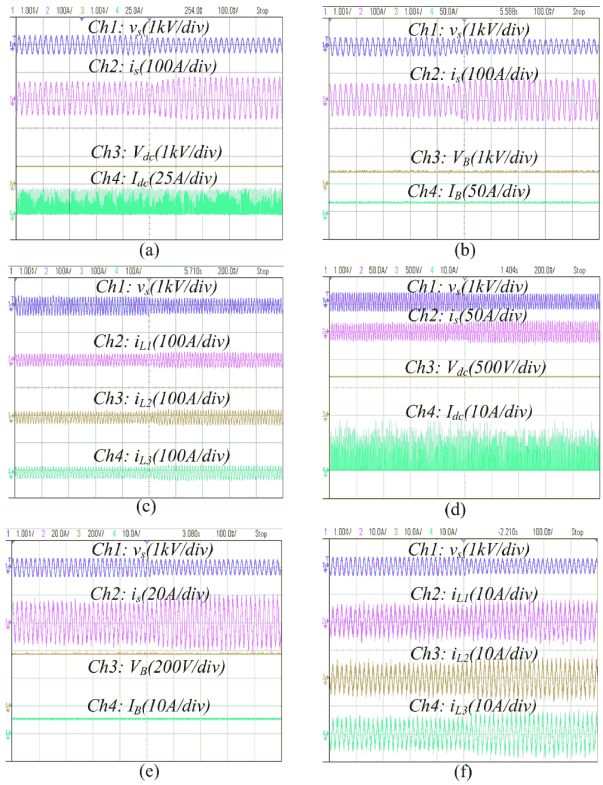

Fig. 8. Experimental dynamic performance with battery load under source voltage disturbance from 230 to 180 V in (a)–(c) CC mode, and (d)–(f) CV mode.

is evaluated and shown in Table I. With the variation in supply voltage from 85–265 V, system operates with almost unity power factor operation.

B. Dynamic Performance of Integrated System in CV and CC Mode

Fig. 8 shows dynamic performance of integrated system against the variation in supply voltage (v_s) and 20% reduction in supply voltage from its nominal voltage (230 V). During changes

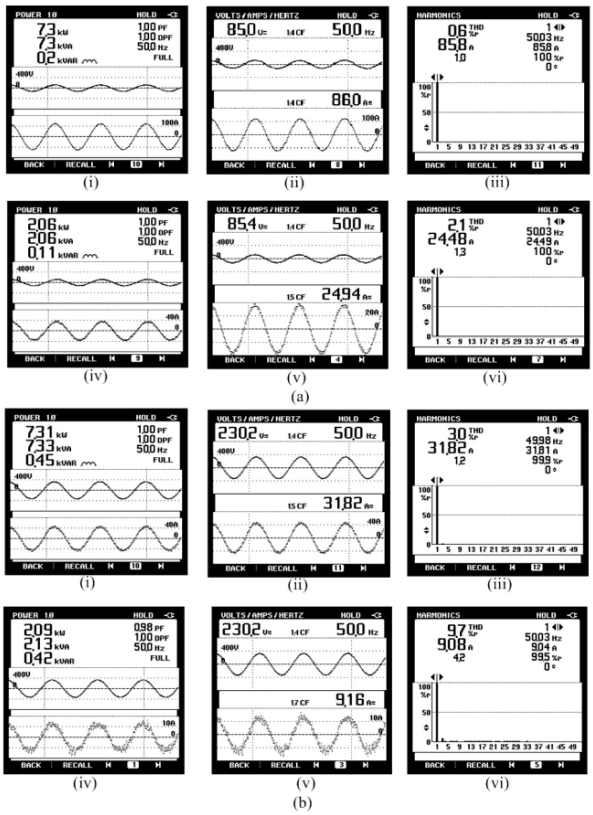

Fig. 9. Performance of converter (a) under 85 V (i) P_s and Q_s (ii) V_s and i_s (iii) harmonic spectra of i_S in CC mode and same for (iv)–(vi) in CV mode, and (b) under 230 V (i)–(iii) in CC and (iv)–(vi) in CV mode.

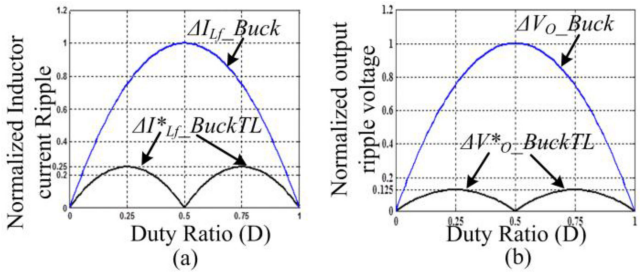

Fig. 10. Performance Comparison of conventional buck and three level buck converter. (a) Normalized input inductor current ripple (D). (b) Normalized output voltage ripple.

in supply voltage from 230 to 180 V, no variation occurred across dc link of VSC, across output voltage of TL converter and battery output voltage of integrated system in both CC and CV modes. Fig. 8 also shows that input inductor currents are disturbed due to disturbance in supply variation. The results of Fig. 9 related with power quality indices of on-board integrated system at rated load condition.

When converter is supplied with ac input voltage of 85 V, total harmonic distortion (THD) in source current are 0.6% in CC mode and 2.1% in CV mode and that of with 230 V, THD in source current are 3% and 9.7% in CC and CV modes respectively, as shown in Fig. 9(a) and (b). These all THD values are within the limits of IEEE-519-2014 standard in CC mode

TABLE II
COMPARATIVE STUDY OF THREE-LEVEL BUCK CONVERTER

Parameters	Conventional buck converter	Three-level Buck converter (D>0.5)	(D<0.5)
Duty Cycle	$D=\frac{V_o}{V_{dc}}=0.57$	$D=\frac{V_o}{V_{dc}}=0.57$	$D=\frac{V_o}{V_{dc}}=0.57$
Switch Voltage Stress	$V_{Sw}=V_{in}=700V$	$V_{Sw}=\frac{V_{in}}{2}=350V$	$V_{Sw}=\frac{V_{in}}{2}=350V$
Switch rating	700V, 20A	350V, 20A	350V, 20A
Inductance value	$L_{crit}=\frac{(1-D)R_o}{2*f}$	$L_{crit}=\frac{(1-D)(2D-1)R_o}{D*4f}$	$L_{crit}=\frac{(1-2D)R_o}{4*f}$
Output capacitor value	$C=\frac{(1-D)}{8f^2L\frac{\Delta V_o}{V_o}}$	$C=\frac{(1-D)(2D-1)}{32f^2L\frac{\Delta V_o}{V_o}};$	$C=\frac{(1-2D)}{32f^2L\frac{\Delta V_o}{V_o}}$
Normalized Ripple Current	$\Delta I^*_{Lf\_Buck}=\frac{\Delta I_{Lf\_Buck}}{\Delta I_{Lf\_Buck\_max}}$	1/4 times of conventional buck converter	1/4 times of conventional buck converter
Normalized ripple output voltage	$\Delta V^*_{Cf\_Buck}=\frac{\Delta V_{Cf\_Buck}}{\Delta V_{Cf\_Buck\_max}}$	1/8 times of conventional buck converter	1/8 times of conventional buck converter
No. of devices	One switch and one diode.	Two switches and two diodes.	
Switching and conduction losses across switch	$P_{Swloss}=\left(\frac{V_{in}I_o}{2}\left(t_r+t_f\right)f_{sw}\right)$ $P_{closs}=I_{SwRMS}{}^2R_{dson}$ $=I_O{}^2DR_{dson}=212R_{dson}$ MOSFET datasheet of 1200V, 20A P_{Swit}= 2.275W P_{cond}= 159W	$P_{Swloss}=\left(\frac{V_{in}I_o}{4}\left(t_r+t_f\right)f_{sw}\right)$ $P_{closs}=I_{SwRMS}{}^2R_{dson}$ $=I_O{}^2DR_{dson}=212R_{dson}$ MOSFET datasheet of 500V, 20A (across one switch) P_{Swit}= 0.6125W P_{cond}= 53W	
Switching and conduction losses across diode	$P_{clossdiode}=V_FI_o(1-D)$ $P_{Swloss}=\left(\frac{V_{in}\times I_{RR}\times t_{RR}\times f_{sw}}{2}\right)$ Diode datasheet of 1200V, 20A P_c=11.18W P_{Sw}= 4.27W	$P_{clossdiode}=V_FI_o(1-D)$ $P_{Swloss}=\left(\frac{V_{in}\times I_{RR}\times t_{RR}\times f_{sw}}{4}\right)$ Diode datasheet of 400V, 20A (across one Diode) P_c=12.04W P_{Sw}= 0.24W	

and CC mode at supply voltage of 85 and 230 V, respectively. It also provides experimental analysis pertaining to power quality features of on-board integrated charging system feeding power to charge the battery for different supply voltages in Table I.

VII. COMPARATIVE STUDY OF THREE LEVEL DC–DC BUCK CONVERTER

A comparative study of the proposed three-level dc–dc converter in integrated system is carried out under buck operation. The intend of this study is to evaluate the performance of aforesaid converter in view of voltage stress, ripple in output voltage, and inductor current and filter size.

Fig. 10 shows, if the ripple inductor current and ripple output voltage of three-level are same as conventional, then size of filter inductor reduces by one-fourth and that of filter output capacitor reduces by one-eighth of conventional converter [24]. Outcome of abovementioned discussions yields that filter components like output inductance and capacitance value reduces because

of effective increase of ripple frequency, as shown in Table II. In addition to above, total switching and conduction loss across two switches of three-level converter are also less as compare to that of conventional converter.

VIII. Conclusion

In this article, mathematical analysis, simulation, design, and real-time implementation of integrated system are carried out. It has following advantages: 1) reduced size of output filter inductor and capacitor; and 2) reduced voltage stress on switches. In addition, interleaved control of IBC in charging mode provides constant dc-link voltage along with maintaining unity power factor. Simulation and experimental results are obtained for various loading conditions in steady-state and transient condition under CC and CV mode. In transient condition of CC and CV mode, irrespective of variation in supply voltage, integrated system is able to provide regulated output voltage to charge battery. The power quality (PQ) indices features power factor (PF) and THD are evaluated at supply side to measure the PQ performance of proposed on-board integrated system. The simulation is validated through real-time implementation of proposed system with same specifications. The experimental results also showed good steady state and transient performance under disturbance of source voltage. Limitations of conventional on-board chargers such cost, weight, and space constraints are avoided using proposed integrated battery charging system.

Appendix

A1. System parameters: (a) for interleaved boost converter: Single-phase supply voltage (v_S) = 230 V, 50 Hz; each three input inductance ($L_1 = L_2 = L_3$) = 10 mH; each two output capacitor ($C_1 = C_2$) = 4700 μF; switching frequency (f_{s1}) = 2.5 kHz; (b) for proposed three level dc–dc converter: input dc voltage (V_{dc}) = 700 V; input inductance (L) = 5 mH; output capacitor (C) = 4700 μF; switching frequency (f_{s2}) = 10 kHz; battery (400 V, 48 Ah.)

A2. Control system parameters: (a) interleaved boost converter two PI voltage controllers gain are $k_{p1} = k_{p2} = 1.2$, $k_{i1} = k_{i2} = 3.5$ and for three PI current controller gains are $k_p = 0.7$ and $k_i = 0.1$. (b) For proposed three level dc–dc converter: PI voltage controller gains are $k_p = 0.01$, $k_i = 3.2$ for constant voltage mode and current controller gains are $k_p = 0.02$, $k_i = 1.5$ for constant current mode operation.

References

[1] M. Ehsani, Y. Gao, S. E. Gay, and A. Emadi, *Modern Electric, Hybrid Electric, and Fuel Cell Vehicles*. Boca Raton, FL, USA: CRC Press, 2005.

[2] A. Y. Saber and G. K. Venayagamoorthy, "One million plug-in electric vehicles on the road by 2015," in *Proc. 12th Int. IEEE Conf. Intell. Transp. Systems*, St. Louis, MO, USA, 2009, pp. 1–7.

[3] A. Emadi, M. Ehsani, and J. M. Miller, *Vehicular Electric Power Systems: Land, Sea, Air, and Space Vehicles*. New York, NY, USA: Marcel Dekker, 2003.

[4] M. Rawson and S. Kateley, "Electric vehicle charging equipment design and health and safety codes," *SAE Trans. California Energy Commission*, vol. 108, no. 6, pp. 3256–3262, Aug. 1998.

[5] C. Botsford and A. Szczepanek, "Fast charging vs. slow charging: Pros and cons for the new age of electric vehicles," presented at the 24th Elect. Veh. Symp., Stavanger, Norway, May 2009, pp. 13–16.

[6] D. Aggeler, F. Canales, H. Zelaya-De La Parra, A. Coccia, N. Butcher, and O. Apeldoorn, "Ultra-fast DC-charge infrastructures for EV-mobility and future smart grids," in *Proc. IEEE PES Innovative Smart Grid Technol. Conf. Eur.*, Gothenberg, 2010, pp. 1–8.

[7] S. Habib, M. M. Khan, K. Hashmi, M. Ali, and H. Tang, "A comparative study of electric vehicles concerning charging infrastructure and power levels," in *Proc. Int. Conf. Frontiers Inf. Technol.*, Islamabad, Pakistan, 2017, pp. 327–332.

[8] L. Solero, "Nonconventional on-board charger for electric vehicle propulsion batteries," *IEEE Trans. Veh. Technol.*, vol. 50, no. 1, pp. 144–149, Jan. 2001.

[9] L. De-Sousa and B. Bouchez, "Combined electric device for powering and charging," International Patent WO 2010/057892 A1, 2010.

[10] M. Grenier, M. G. Hosseini Aghdam, and T. Thiringer, "Design of on-board charger for plug-in hybrid electric vehicle," in *Proc. 5th IET Int. Conf. Power Electron., Mach. Drives*, Brighton, U.K., 2010, pp. 1–6.

[11] M. Yilmaz and P. T. Krein, "Review of battery charger topologies, charging power levels, and infrastructure for plug-in electric and hybrid vehicles," *IEEE Trans. Power Electron.*, vol. 28, no. 5, pp. 2151–2169, May 2013.

[12] F. Musavi, M. Edington, W. Eberle, and W. G. Dunford, "Evaluation and efficiency comparison of front end AC-DC plug-in hybrid charger topologies," *IEEE Trans. Smart Grid*, vol. 3, no. 1, pp. 413–421, Mar. 2012.

[13] M. A. Fasugba and P. T. Krein, "Gaining vehicle-to-grid benefits with unidirectional electric and plug-in hybrid vehicle chargers," in *Proc. IEEE Vehicle Power Propulsion Conf.*, Chicago, IL, USA, 2011, pp. 1–6.

[14] Y. Lee, A. Khaligh, and A. Emadi, "Advanced integrated bi-directional AC/DC and DC/DC converter for plug-in hybrid electric vehicles," *IEEE Trans. Veh. Technol.*, vol. 58, no. 3, pp. 3970–3980, Oct. 2009.

[15] O. Garcia, P. Zurnel, A. de Castro, and A. Cobos, "Automotive dc–dc bidirectional converter made with many interleaved buck stages," *IEEE Trans. Power Electron.*, vol. 21, no. 3, pp. 578–586, May 2006.

[16] D. C. Erb, O. C. Onar, and A. Khaligh, "Bi-directional charging topologies for plug-in hybrid electric vehicles," in *Proc. 25th Annu. IEEE Appl. Power Electron. Conf. Expo.*, Palm Springs, CA, USA, 2010, pp. 2066–2072.

[17] S. Haghbin *et al.*, "Integrated chargers for EV's and PHEV's: Examples and new solutions," in *Proc. XIX Int. Conf. Electrical Mach.*, Rome, 2010, pp. 1–6.

[18] S. Lacroix, E. Laboure, and M. Hilairet, "An integrated fast battery charger for electric vehicle," in *Proc. IEEE Vehicle Power Propulsion Conf.* Lille, 2010, pp. 1–6.

[19] D. Thimmesch, "An SCR inverter with an integral battery charger for electric vehicles," *IEEE Trans. Ind. Appl.*, vol. IA-21, no. 4, pp. 1023–1029, Jul. 1985.

[20] W. E. Rippel, "Integrated traction inverter and battery charger apparatus," U.S. Patent 4920475, Apr. 1990.

[21] W. E. Rippel and A. G. Cocconi, "Integrated motor drive and recharge system," U.S. Patent 5099186, Mar. 1992.

[22] E. H. Ismail, M. A. Al-Saffar, and A. J. Sabzali, "High conversion ratio DC–DC converters with reduced switch stress," *IEEE Trans. Circuits Sys. I: Regular Papers*, vol. 55, no. 7, pp. 2139–2151, Aug. 2008.

[23] X. Zhou, S. Lukic, S. Bhattacharya, and A. Huang, "Design and control of grid-connected converter in bi-directional battery charger for Plug-in hybrid electric vehicle application," in *Proc. IEEE Vehicle Power Propulsion Conf.*, Dearborn, MI, USA, 2009, pp. 1716–1721.

[24] X. Ruan, B. Li, Q. Chen, S. Tan, and C. K. Tse, "Fundamental considerations of three-level DC–DC Converters: Topologies, analyses, and control," *IEEE Trans. Circuits Sys. I, Regular Papers*, vol. 55, no. 11, pp. 3733–3743, Dec. 2008.

[25] X. Ruan, B. Li, and Q. Chen, "Three-level converters-a new approach for high voltage and high power DC-to-DC conversion," in *Proc. IEEE 33rd Annu. IEEE Power Electron. Specialists Conf.*, Australia, 2002, vol. 2, pp. 663–668.

[26] B. Singh, K. Al-Haddad, and A. Chandra, "A review of active filters for power quality improvement," *IEEE Trans. Ind. Electron.*, vol. 46, no. 5, pp. 960–971, Oct. 1999.

[27] D. Bozalakov, B. Meersman, A. Bottenberg, J. Rens, J. Desmet, and L. Vandevelde, "Dc-bus voltage balancing controllers for split dc-link four-wire inverters and their impact on the quality of the injected currents," *CIRED - Open Access Proc. J.*, vol. 2017, no. 1, pp. 564–568, Oct. 2017.

[28] M. Farhadi, M. T. Fard, M. Abapour, and M. T. Hagh, "DC–AC converter-fed induction motor drive with fault-tolerant capability under open- and short-circuit switch failures," *IEEE Trans. Power Electron.*, vol. 33, no. 2, pp. 1609–1621, Feb. 2018.

Jyoti Gupta (Student Member, IEEE) received the B.Tech. degree in electrical engineering from Swami Keshvanand Institute of Technology, Management, and Gramothan, Jaipur, India, in 2013, and the M.Tech. degree in power systems from Rajasthan Technical University, Kota, India, in 2017. She is currently working toward the Ph.D. degree with the Department of Electrical Engineering, Sardar Vallabhbhai National Institute of Technology, Surat, India.

She was a Lecturer with the Department of Electrical, Apex Institute of Engineering and Technology, Jaipur, India, from 2014 to 2015. Her research interests include dc–dc converters, power quality, and battery charging for EV applications.

Rakesh Maurya (Member, IEEE) received B. Tech. degree in electrical engineering from the Kamla Nehru Institute of Technology, Sultanpur, India, in 1998, and the M. Tech. degree in power electronics and electric drive and the Ph.D. degree in electrical engineering from the Indian Institute of Technology Roorkee, Roorkee, India, in 2002 and 2014, respectively.

He is currently an Associate Professor with the Department of Electrical Engineering, Sardar Vallabhbhai National Institute of Technology, Surat, India. In last five years, he has authored and coauthored more than 35 SCI/SCIE research papers in journals of international repute, particularly IEEE Transactions, IETs-UK, and *Elsevier*, *Taylor & Francis,* and many conference papers. His current research interests include design of switching power converters, high power factor ac–dc converters, hybrid output converters, improved power quality converters for battery charging applications, power quality problems, advanced electric drives, and applications of real-time simulator for the control of power converters.

Dr. Maurya is Life Member of the System Society of India.

Sabha Raj Arya (Senior Member, IEEE) received the B.E. degree in electrical engineering from the Government Engineering College, Jabalpur, India, in 2002, the M.Tech. degree in power electronics from Motilal National Institute of Technology, Allahabad, Allahabad, India, in 2004, and the Ph.D. degree in electrical engineering from the Indian Institute of Technology Delhi, New Delhi, India, in 2014.

He is an Assistant Professor with the Department of Electrical Engineering, Sardar Vallabhbhai National Institute of Technology, Surat, India, where he was promoted as Associate Professor. He has authored and coauthored more than 100 research paper in internal national journals and conferences in field of electrical power quality. His research interests include power electronics, power quality, design of power filters, and distributed power generation.

Prof. Arya is the recipient of the INAE Young Engineer Award from the Indian National Academy of Engineering, and POSOCO Power System Award from the Power Grid Corporation of India, in 2014. He also received Amit Garg Memorial Research Award-2014 from IIT Delhi, from the high impact publication in a quality journal during the session 2013–2014. He is an Associate Editor for the *IET (U.K.) Renewable Power Generation.*